ELSEVIER

Journal of Organometallic Chemistry 580 (1999) 328–338

Journal of Organometallic Chemistry

Synthesis, reactions and X-ray crystal structures of metallacrown ethers with unsymmetrical bis(phosphinite) and bis(phosphite) ligands derived from 2-hydroxy-2′-(1,4-bisoxo-6-hexanol)-1,1′-biphenyl

Maheswaran Hariharasarma, Charles H. Lake, Charles L. Watkins, Gary M. Gray *

Department of Chemistry, CHEM 201 UAB Station, The University of Alabama at Birmingham, 901 South 14th Street, Birmingham, AL 35294-1240, USA

Received 28 September 1998

Abstract

Chlorodiphenylphosphine and 2,2′-biphenylylenephosphorochloridite react with 2-hydroxy-2′-(1,4-bisoxo-6-hexanol)-1,1′-biphenyl to yield the new α,ω-bis(phosphorus-donor)-polyether ligands, 2-$Ph_2PO(CH_2CH_2O)_2$–$C_{12}H_8$-2′-$OPPh_2$ (**1**) and 2-(2,2′-$O_2C_{12}H_8$)$P(CH_2CH_2O)_2$–$C_{12}H_8$-2′-P(2,2′-$O_2C_{12}H_8$) (**2**). These ligands react with $Mo(CO)_4$(nbd) to form the monomeric metallacrown ethers, *cis*-$Mo(CO)_4${2-$Ph_2PO(CH_2CH_2O)_2$–$C_{12}H_8$-2′-$OPPh_2$} (*cis*-**3**) and *cis*-$Mo(CO)_4${2-(2,2′-$O_2C_{12}H_8$)$P(CH_2CH_2O)_2$–$C_{12}H_8$-2′-P(2,2′-$O_2C_{12}H_8$)} (*cis*-**4**), in good yields. The X-ray crystal structures of *cis*-**3** and *cis*-**4** are significantly different, especially in the conformation of the metal center and the adjacent ethylene group. The very different ^{13}C-NMR coordination chemical shifts of this ethylene group in *cis*-**3** and *cis*-**4** suggest that the solution conformations of these metallacrown ethers are also quite different. Both metallacrown ethers undergo *cis–trans* isomerization in the presence of $HgCl_2$. Although the *cis–trans* equilibrium constants for the isomerization reactions are nearly identical, the isomerization of *cis*-**3** is more rapid. Phenyl lithium reacts with *cis*-**3** to form the corresponding benzoyl complexes but does not react with either *trans*-**3** or *cis*-**4**. Both the slower rate of *cis–trans* isomerization of *cis*-**4** and its lack of reaction with PhLi are consistent with weaker interactions between the hard metal cations and the carbonyl oxygens in both *trans*-**3** and *cis*-**4**. © 1999 Elsevier Science S.A. All rights reserved.

Keywords: Metallcrown ethers; Phosphite; Phosphinite; Carbonyl activation

1. Introduction

Metallacrown ethers are formed when α,ω-bis(phosphorus-donor)polyether ligands chelate soft transition metals. These complexes bind alkali metal cations to form hard–soft bimetallic complexes with the strength of the binding depending on both the ring size and conformation [1–3]. This ability is of interest because hard–soft bimetallic complexes can function as highly active catalysts for olefin hydroformylation reactions [4].

Almost all of the metallacrown ethers that have been studied to date are derived from polyethylene glycols and thus have symmetrical and conformationally flexible metallacrown ether rings. Metallacrown ethers with unsymmetrical and conformationally rigid metallacrown ether rings are of interest because they could interact quite differently with hard metal cations. The recently synthesized polyether diol, 2-hydroxy-2′-(1,4-bisoxo-6-hexanol)-1,1′-biphenyl is a promising precursor for such metallacrown ethers [5]. An added advantage of this precursor is that the methylene ^{1}H- and ^{13}C{^{1}H}-NMR resonances are well resolved, unlike those of the polyethylene glycols. This suggests that NMR spectroscopy could be used to study the solution

* Corresponding author.
E-mail address: gmgray@uab.edu (G.M. Gray)

0022-328X/99/$ - see front matter © 1999 Elsevier Science S.A. All rights reserved.
PII: S0022-328X(98)01170-X

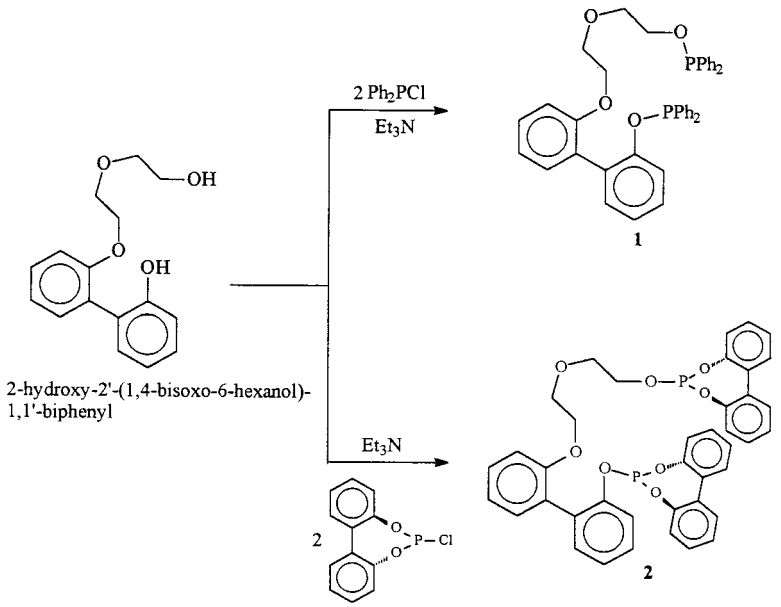

Fig. 1. Synthetic scheme for the bis(phosphorus donor)-polyether ligands, **1** and **2**.

state conformational features of the metallacrown ethers derived from this precursor.

In this paper, we report the synthesis and characterization of α,ω-bis(phosphinite)- and α,ω-bis(phosphite)-polyether ligands derived from 2-hydroxy-2′-(1,4-bisoxo-6-hexanol)-1,1′-biphenyl. The *cis*-$Mo(CO)_4$ complexes of both ligands have been prepared, and the solution state conformational features of the complex with the bis(phosphite)-polyether ligand have been investigated using one- and two-dimensional NMR spectroscopic techniques. The X-ray crystal structures of both complexes have been determined, and pertinent features of these structures are described. The reactions of both complexes with both PhLi and $HgCl_2$ have also been studied.

2. Results and discussion

2.1. Synthesis and NMR characterization of the ligands

The ligands, 2-$Ph_2PO(CH_2CH_2O)_2$–$C_{12}H_8$-2′-$OPPh_2$ (**1**) and 2-(2,2′-$O_2C_{12}H_8$)$P(CH_2CH_2O)_2$–$C_{12}H_8$-2′-$P(2,2'\text{-}O_2C_{12}H_8)$ (**2**) were prepared by the reactions of 2-hydroxy-2′-(1,4-bisoxo-6-hexanol)-1,1′-biphenyl with chlorodiphenylphosphine and 2,2′-biphenylylenephosphorochloridite ester, respectively, in the presence of triethylamine (Fig. 1). The $^{31}P\{^1H\}$-, $^{13}C\{^1H\}$- and ^1H-NMR spectra of the crude ligands contained no unexplained resonances, and the crude ligands were used in the syntheses of the metallacrown ethers.

The NMR spectra of **1** and **2** show no unexpected features. Two singlets are observed in the $^{31}P\{^1H\}$-NMR spectrum of each ligand due to the inequivalent phosphorus nuclei. The chemical shifts of these singlets are assigned on the basis of ^1H-coupled ^{31}P-NMR spectra and by comparison with the chemical shifts of the ^{31}P-NMR resonances of ligands with similar phosphorus environments [6]. The ^{13}C-NMR spectrum of each ligand exhibits well-resolved resonances for all of the methylene carbons. The resonances of the carbons two and three bonds from the phosphorus ($\underline{C}H_2OP$ and $\underline{C}H_2CH_2OP$, respectively) are doublets and are readily assigned by their chemical shifts and the relative values of the $|^nJ(PC)|$ coupling constants. The assignment of the resonances for the carbons five and six bonds from the phosphorus ($\underline{C}H_2OAr$ and $\underline{C}H_2CH_2OAr$, respectively) is consistent with the assignment made for these resonances in *cis*-**4**. The ^1H-NMR spectrum of each ligand exhibits four resonances in the 3.3–4.1 ppm region, indicating that the protons attached to each methylene carbon are chemically equivalent. No attempt was made to assign these resonances.

2.2. Synthesis and NMR characterization of the metallacrown ethers

We initially prepared both $Mo(CO)_4\{2\text{-}Ph_2PO(CH_2CH_2O)_2\text{–}C_{12}H_8\text{-}2'\text{-}OPPh_2\}$ (**3**) and $Mo(CO)_4\{2\text{-}(2,2'\text{-}O_2C_{12}H_8)P(CH_2CH_2O)_2\text{–}C_{12}H_8\text{-}2'\text{-}P(2,2'\text{-}O_2C_{12}H_8)\}$ (**4**) in good yields by the reactions of $Mo(CO)_4\{nbd\}$ with ligands **1** and **2**, respectively, under relatively high-dilution conditions (Fig. 2). Both complexes were initially colorless, but **4** became colored when stored in the air in the solid state for several days. This behavior is unusual as most $Mo(CO)_4$-

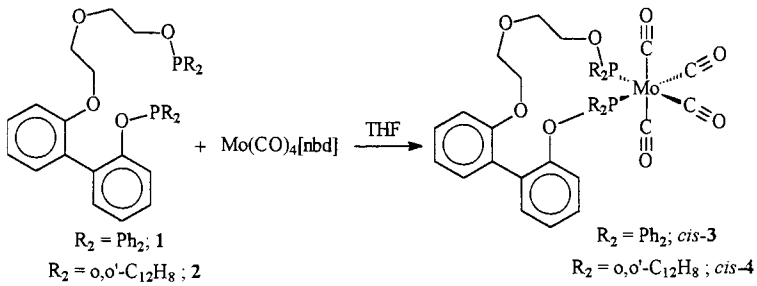

Fig. 2. Synthetic scheme for the metallacrown ether complexes, *cis*-**3** and *cis*-**4**.

{bis(phosphite)} complexes are relatively air stable. Storing this complex in the dark under nitrogen eliminated this problem.

The $^{31}P\{^{1}H\}$-NMR spectrum of **4** displays a single AX pattern as expected. Both the coordination chemical shifts of these resonances (ca. 30 ppm) and the $|^{2}J(PP')|$ coupling constant of 48 Hz indicate that only the *cis* isomer of **4** (*cis*-**4**) is present. In contrast, the ^{31}P-NMR spectrum of **3** displays two AX spectral patterns. Both the coordination chemical shifts and coupling constants demonstrate that the major product (ca. 30 ppm, 34 Hz) is the *cis* isomer of **3** (*cis*-**3**) and the minor product (ca. 47 ppm, 89 Hz) is the *trans* isomer of **3** (*trans*-**3**).

The ^{13}C-NMR spectra of *cis*-**3** and *cis*-**4** exhibit two interesting features. The first is that well resolved resonances are observed for all four carbonyls, which is extremely unusual for *cis*-$Mo(CO)_4$(P-donor ligand)$_2$ complexes. The carbonyls *trans* to the phosphorus-donor groups are chemically inequivalent because the two phosphorus-donor groups in the ligands are different. The inequivalence of the carbonyls *cis* to both phosphorus-donor groups cannot be due to this and instead must be due to an unsymmetrical arrangement of the metallacrown ether ring relative to the plane containing the molybdenum and the two phosphorus-donor groups.

A second interesting aspect of the ^{13}C-NMR spectra of *cis*-**3** and *cis*-**4** is that the coordination chemical shifts of equivalent methylene ^{13}C-NMR resonances in *cis*-**3** and *cis*-**4** are quite different. The largest differences are in the coordination chemical shifts of the $\underline{C}H_2OP$ resonances (3.7 ppm upfield from that of the free ligand, **1**, in *cis*-**3** vs. 3.8 ppm downfield of that of the free ligand, **2**, in *cis*-**4**). These shifts cannot be explained by electronic effects of the phosphorus donor substituents and must instead be due to different average solution conformations of the metallacrown ether carbons. This hypothesis is consistent with the fact that the metallacrown ether rings of *cis*-**3** and *cis*-**4** have very different solid state conformations at the $\underline{C}H_2OP$ carbon (see Section 2.4).

2.3. Solution conformations of the metallacrown ethers

To gain more insight into the solution conformation of *cis*-**4**, we have completely assigned the ^{1}H- and ^{13}C-NMR resonances of the methylene groups and calculated the geminal and vicinal H–H coupling constants. We would also have liked to carry out this same analysis for *cis*-**3**, however, unlike *cis*-**4**, *cis*-**3** does not exhibit well-resolved resonances for all of the methylene carbons and protons. In addition, *cis*-**3** slowly isomerizes to *trans*-**3** in solution, which prevents accurate 2-D NMR spectra from being obtained. The $^{13}C\{^{1}H\}$-NMR resonances of this complex were assigned by comparison with those of *cis*-**4**.

The $^{13}C\{^{1}H\}$- and ^{1}H-NMR resonances of the methylenes in *cis*-**4** were assigned using a variety of two-dimensional NMR techniques [7]. A $^{31}P\{^{1}H\}$ HETCOR NMR experiment was used to assign the resonances of the methylenes closest to the phosphorus ($\underline{C}H_2OP$; H4′ & H4) because these are the only methylene protons that are coupled to the phosphorus. A phase-sensitive $^{1}H-^{1}H$ NOESY NMR experiment was used to assign the proton resonances of the methylene closest to the 2,2′-biphenoxy group ($\underline{C}H_2OAr$; H1 and H1′) because both protons show NOESY contacts to the 3 proton of the 2,2′-biphenoxy group. A $^{1}H-^{1}H$ COSY-45 NMR experiment was run to determine the remaining $^{1}H-^{1}H$ connectivity, and the $^{1}H-^{13}C$ connectivity was then determined using a $^{13}C\{^{1}H\}$ HETCOR NMR experiment.

The magnitudes of the geminal, $|^{2}J(H,H)|$, and vicinal, $|^{3}J(H,H)|$, coupling constants of the diastereotopic OCH_2CH_2O fragments of *cis*-**4** (Fig. 3) provide significant insight into the average conformations [7] about the OCH_2CH_2O groups in the metallacrown ether ring. The geminal coupling constants are ca. 12 Hz for both OCH_2CH_2O groups, consistent with the tetrahedral geometry around each methylene carbon. One moderate vicinal coupling constant of 7–8 Hz and three small vicinal coupling constants of 3–4 Hz are observed for each of the OCH_2CH_2O groups. The magnitudes of the vicinal coupling constants indicate that the average solution conformation about the C–C bonds in each of

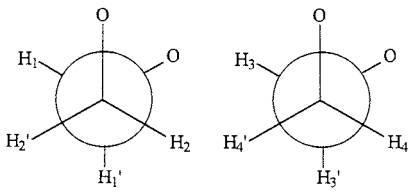

$\lvert^2J(H_1,H_1')\rvert$ = 10.7 Hz	$\lvert^2J(H_3,H_3')\rvert$ = 12.6 Hz
$\lvert^2J(H_2,H_2')\rvert$ = 11.5 Hz	$\lvert^2J(H_4,H_4')\rvert$ = not observed
$\lvert^3J(H_1,H_2)\rvert$ = 8.0 Hz	$\lvert^3J(H_3,H_4)\rvert$ = 6.7 Hz
$\lvert^3J(H_1,H_2')\rvert$ = 2.8 Hz	$\lvert^3J(H_3,H_4')\rvert$ = 3.5 Hz
$\lvert^3J(H_1',H_2)\rvert$ = 3.0 Hz	$\lvert^3J(H_3',H_4)\rvert$ = 3.7 Hz
$\lvert^3J(H_1',H_2')\rvert$ = 3.5 Hz	$\lvert^3J(H_3',H_4')\rvert$ = 3.7 Hz

Fig. 3. The magnitudes of geminal $|^2J(H,H))|$ and vicinal coupling constants $|^3J(H,H)|$ of the diastereotopic OCH_2CH_2O fragments of *cis*-**4**.

the OCH_2CH_2O groups in the metallacrown ether ring is *gauche*. *Gauche* conformations about these bonds are also observed in the solid state structure of *cis*-**4**, as discussed below.

2.4. Solid-state structures of the complexes

The molecular structures of *cis*-**3** and *cis*-**4** are shown in Figs. 4 and 5, respectively. These structures are of interest because, unlike other metallacrown ethers whose structures have been reported, these metallacrown ethers are unsymmetrical and sterically crowded.

The coordination geometry of the molybdenum in each complex is a distorted octahedron. The distortion is significantly greater in *cis*-**3** than in *cis*-**4** as indicated

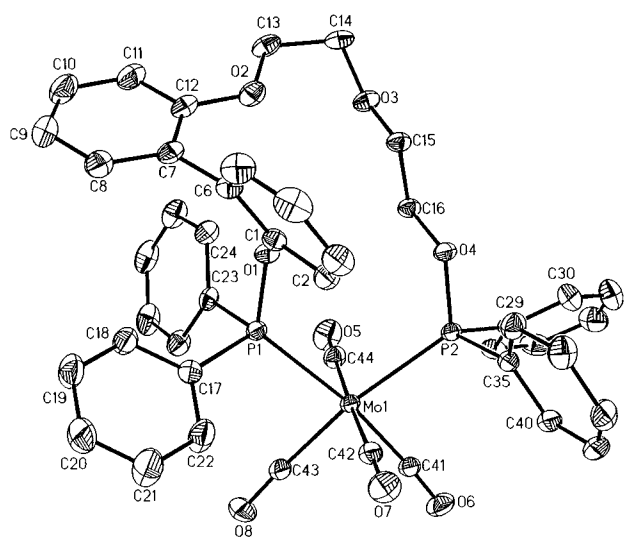

Fig. 4. ORTEP drawing of the molecular structure of *cis*-**3**. The hydrogens are omitted for clarity, and the thermal ellipsoids are drawn at the 20% probability level.

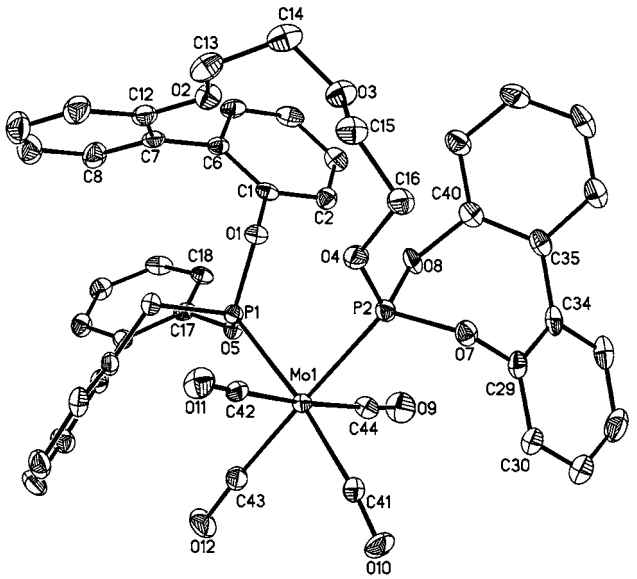

Fig. 5. ORTEP drawing of the molecular structure of *cis*-**4**. The hydrogens are omitted for clarity, and the thermal ellipsoids are drawn at the 20% probability level.

by very different phosphorus–molybdenum–phosphorus bond angles (102.4(1)° in *cis*-**3** vs. 91.7(1)° in *cis*-**4**). This suggests that the diphenylphosphinite groups in *cis*-**3** are sterically more demanding than are the dibenzo[*d*,*f*][1,3,2]dioxaphosphepin groups in *cis*-**4**. This conclusion is consistent with the expected cone angles of phosphorus-donor groups [8–11]. The lack of steric strain in *cis*-**4** is also indicated by the dihedral angles of the 2,2′-biphenyl groups of the dibenzo[*d*,*f*][1,3,2]-dioxaphosphepin groups, 44.6 and 47.8°, which are very similar to each other and are also similar to those in other dibenzo[*d*,*f*][1,3,2]dioxaphosphepin ligands [12].

The conformations of the metallacrown ether rings in *cis*-**3** and *cis*-**4** are the most interesting aspects of the structures. The biphenyl groups and the adjacent OCH_2CH_2O groups have similar confirmations in the two complexes. The dihedral angles between mean least square planes of the phenylene rings in *cis*-**3** and *cis*-**4** are quite similar (65.3 and 63.1°, respectively) and are in the expected range for *ortho*-disubstituted biphenyl compounds [12]. Moreover, *gauche* conformations for the –O2–C13–C14–O3– groups adjacent to the biphenyl group are observed in both *cis*-**3** (67.3°) and *cis*-**4** (− 68.2°). In contrast, the metal centers and the adjacent OCH_2CH_2O groups have very different conformations in *cis*-**3** and *cis*-**4**. In *cis*-**3**, the –O3–C15–C16–O4– group has a *trans anti* conformation (178.2°) while in *cis*-**4**, it has a *gauche* conformation (− 68.4°). These differences demonstrate that the phosphorus substituents have a significant influence on the solid state conformations of the complexes. It is interesting to note that the conformations of the OCH_2CH_2O groups in *cis*-**4** are the same in the solid state and in the average solution state conformation of the metallacrown ether.

2.5. Cis–trans isomerization equilibria of the metallacrown ethers

As discussed above, the reaction of $Mo(CO)_4$(nbd) and **1** in THF under moderately high dilution conditions yields a mixture of *cis*-**3** and *trans*-**3**. Because $Mo(CO)_4$(nbd) reacts with phosphorus-donor ligands to exclusively form *cis* isomers, the *trans*-**3** must form via isomerization of *cis*-**3**. To prove this, we carried out the reaction of **1** and $Mo(CO)_4$(nbd) in hexanes. Both **1** and $Mo(CO)_4$(nbd) are sparingly soluble in hexanes while both *cis*-**3** and *trans*-**3** are insoluble. Under these conditions, only the *cis*-**3** precipitates from the reaction mixture. Surprisingly, we did not observe formation of oligomeric complexes in spite of the fact that the reaction was carried out with relatively high concentrations of **1** and $Mo(CO)_4$(nbd). This suggests that the steric constraints in **1** favor formation of monomeric metallacrown ethers.

The fact that *cis*-**3** readily undergoes isomerization while *cis*-**4** does not suggests that the phosphorus substituents have a significant effect on this isomerization. To better understand this phenomenon, we have studied the $HgCl_2$ catalyzed isomerizations [13] of *cis*-**3** and *cis*-**4**, shown in Fig. 6. These studies were carried out by adding solid $HgCl_2$ to chloroform-d_1 solutions of the complexes in a mole ratio of 1:100. For *cis*-**3**, the *cis–trans* equilibrium is established in less than 5 min, which is the time needed to add solid $HgCl_2$ to a freshly prepared chloroform-d_1 solution of *cis*-**3**, shake the mixture vigorously, and record a non-quantitative ^{31}P-NMR spectrum. The equilibrium constant for the reaction at 294 K, calculated using $K_{eq} = [trans\text{-}3]/[cis\text{-}3]$, is 3.6 ± 0.4 [14]. For *cis*-**4**, the equilibrium is reached in 20 min. The equilibrium constant for the reaction at 294 K, calculated using $K_{eq} = [trans\text{-}3]/[cis\text{-}3]$, is 4.2 ± 0.4.

The rates of the $HgCl_2$-catalyzed *cis–trans* isomerization for the two complexes are quite different, with that of *cis*-**3** being significantly faster. The relative rates of *cis–trans* isomerization are consistent with the fact that only *cis*-**3** is observed to isomerize in solution in the absence of $HgCl_2$. Because the isomerization presumably occurs via coordination of the $HgCl_2$ to both the metallacrown ether and a carbonyl oxygens, the relative rates of isomerization suggest that the $HgCl_2$ does not interact as strongly with the carbonyl oxygens in *cis*-**4**.

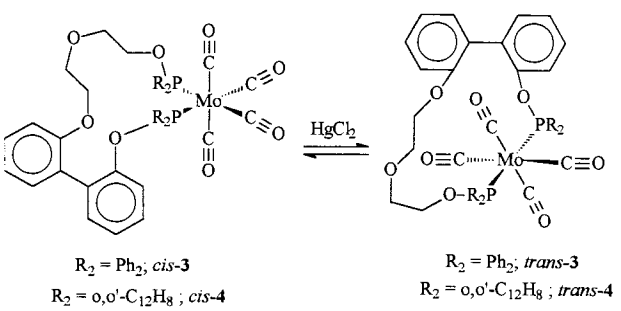

Fig. 6. $HgCl_2$ catalyzed *cis–trans* isomerization of the *cis*-metallacrown ethers, *cis*-**3** and *cis*-**4**.

In contrast to the differences in the rates of the *cis–trans* isomerization reactions of *cis*-**3** and *cis*-**4**, the *cis–trans* equilibrium constants for the two metallacrown ethers are not statistically different (assuming a 5% error in the integration of the two resonances in the quantitative ^{31}P-NMR spectra). The similarity of the equilibrium constants indicates that they are not strongly affected by the phosphorus substituents. However, these equilibrium constants are significantly larger than those reported for *cis*-$Mo(CO)_4\{Ph_2P(CH_2CH_2O)_4CH_2CH_2PPh_2$-*P*,*P*′}, and *cis*-$Mo(CO)_4\{Ph_2PCH_2CH_2OCH_2CH_2O$-1,2-$C_6H_4$–$OCH_2CH_2OCH_2CH_2PPh_2$-*P*,*P*′}, 1.0 and 0.23, respectively [13]. This indicates that the magnitudes of the *cis–trans* equilibrium constants are quite sensitive to the nature of the metallacrown ether ring. The fact that metallacrown ethers with a bulky 2,2-biphenoxy group adjacent to the phosphorus have larger *cis–trans* equilibrium constants than those with less bulky groups adjacent to the phosphorus is not surprising because the position of equilibrium for *cis–trans* isomerization in *cis*-$Mo(CO)_4$(phosphorus-donor)$_2$ complexes is known to parallel the steric requirement of the phosphorus-donor ligand [10,11].

2.6. Reactions of metallacrown ethers with PhLi

Previous studies by Powell's group [1] have established that the coordination of Li^+ to both a metallacrown ether and a carbonyl oxygen activates the *cis*-carbonyl ligands in *cis*-$Mo(CO)_4$-metallacrown ethers to nucleophilic attack by PhLi reagents. This mechanism is similar to that which we have proposed for the $HgCl_2$ catalyzed *cis–trans* isomerization of the metallacrown ethers [13]. On the basis of the difference in the rates of the *cis–trans* isomerization reactions of *cis*-**3** and *cis*-**4**, it seemed likely that these metallacrown ethers should also react differently with PhLi, and this is indeed the case. When PhLi is added to a benzene-d_6 solution of *cis*-**4**, no reaction is observed. In contrast, when an excess of PhLi is added to a benzene-d_6 solution mixture of *cis*-**3** (major) and *trans*-**3** (minor), the solution first becomes orange, and then an orange solid slowly precipitates. The IR spectrum of the orange solution contains three new, strong CO absorptions at 1942, 1873 and 1838 cm^{-1} (80–100 cm^{-1} less than the absorptions due to *cis*-**3**). The ^{31}P-NMR spectrum of the orange solution contains a new AX spectral pattern that is ca. 20 ppm downfield from that of *cis*-**3** in addition to the unchanged AX pattern of *trans*-**3**. These

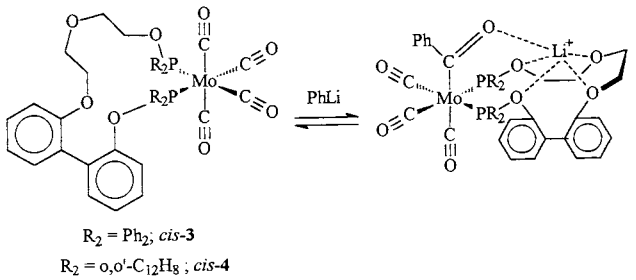

Fig. 7. Reaction of PhLi with the *cis*-metallacrown ethers, *cis*-**3** and *cis*-**4**.

data indicate that PhLi reacts with *cis*-**3** to give *fac*-$Mo(CO)_3(PhC(O))\{2\text{-}Ph_2PO(CH_2CH_2O)_2\text{-}C_{12}H_8\text{-}2'\text{-}OPPh_2\}$ as shown in Fig. 7. A unique aspect of this reaction is that although *cis*-**3** has two chemically inequivalent *cis*-carbonyls that can potentially react with PhLi, only a single product is formed. This suggests that one of the *cis*-carbonyls preferentially reacts with the PhLi.

The nature of the metallacrown ether obviously has a dramatic effect on its ability to react with PhLi. Powell has proposed that the difference in the reactivities of the carbonyl ligands in bis(phosphite) metallacrown ethers such as *cis*-**4** and bis(phosphinite) metallacrown ethers such as *cis*-**3** is due to the fact that phosphites are poorer electron donors than phosphinites [1d]. However, Powell has also demonstrated that PhLi can coordinate to phosphite oxygens [1f]. This could prevent carbonyl activation in the same manner that additional ether oxygens do [1]. Our solution and conformational studies have now demonstrated that the phosphorus substituents also have a dramatic effect on the solution and solid state conformations of the metallacrown ethers. These differences could also affect the ability of a Li^+ to coordinate to a carbonyl ligand.

The fact that *trans*-**3** does not react with PhLi cannot be due to electronic or coordination effects and must be due to differences in the conformations of *cis*-**3** and *trans*-**3**. Our studies of the structures of *cis*- and *trans*-metallacrown ethers with bis(phosphine)polyether ligands have demonstrated that ether oxygens in the *trans*-metallacrown ethers are significantly farther apart than they are in the *cis* metallacrown ethers with the same ligands [13]. This suggests that *trans*-**3** does not react with PhLi because the ether oxygens are unable to adopt a conformation that allows Li^+ to coordinate to both the metallacrown ether oxygens and a carbonyl oxygen.

3. Experimental

All one-dimensional $^{31}P\{^1H\}$-, $^{13}C\{^1H\}$- and ^1H-NMR spectra of the ligands and complexes were recorded using a Bruker ARX-300 NMR spectrometer with a quad (^1H-, ^{13}C-, ^{19}F-, ^{31}P-) 5 mm probe. The $^{31}P\{^1H\}$-NMR spectra were referenced to external 85% phosphoric acid, while both the $^{13}C\{^1H\}$- and the ^1H-NMR spectra were referenced to internal $SiMe_4$. In all cases, downfield was treated as positive. Quantitative ^{31}P-NMR spectra of chloroform-*d* solutions of the complexes were acquired using an inverse-gated 30° pulse sequence with a 30-s delay between acquisitions. Two-dimensional $^1H-^1H$ COSY-45, $^{31}P\{^1H\}$ HETCOR, $^{13}C\{^1H\}$ HETCOR and $^1H-^1H$ NOESY spectra of 0.2 M chloroform-*d* solutions of the complexes were recorded using a Bruker DRX-400 NMR spectrometer. All two-dimensional data were processed using standard Bruker programs. The IR spectra of dilute benzene solutions of the complexes in the 2200–1800 cm^{-1} region were taken on a Bruker Vector 22 FTIR spectrometer. Elemental analyses were performed by Atlantic Microlabs, Norcross, GA. A solvent of crystallization is included in a calculated analysis only if the solvent was observed in the NMR spectrum of the analytical sample.

All reactions and purification procedures were carried out under high-purity nitrogen. All starting materials were reagent grade and were used as received. THF was distilled from sodium/benzophenone under high-purity nitrogen. Triethylamine was distilled from calcium hydride prior to use. Deuterated NMR solvents (chloroform-*d*, benzene-d_6 and THF-d_8) were opened and handled under a nitrogen atmosphere at all times. The starting materials, 2-hydroxy-2′-(1,4-bisoxo-6-hexanol)-1,1′-biphenyl [5], *cis*-$Mo(CO)_4$(nbd) [15], and 2,2′-biphenylylene phosphorochloridite ester [16], were synthesized using literature procedures. Phenyllithium solution was purchased from Aldrich Chemical Company and used from newly opened bottles. All complexes were stored in the dark under dry nitrogen.

3.1. 2-$Ph_2PO(CH_2CH_2O)_2$–$C_{12}H_8$-2′-$OPPh_2$ (1)

A solution of 4.44 g (20.0 mmol) of chlorodiphenylphosphine in 75 ml of THF was added to a solution of 2.74 g (10.0 mmol) of 2-hydroxy-2′-(1,4-bisoxo-6-hexanol)-1,1′-biphenyl and 2.80 ml (20.0 mmol) of triethylamine in 100 ml of THF at room temperature (r.t.). The mixture was stirred for 15 h and then was filtered to remove the triethylamine hydrochloride precipitate. The filtrate was evaporated to dryness to give 6.23 g (96.9%) of crude **1** as a colorless oil. $^{31}P\{^1H\}$-NMR (chloroform-*d*): δ 115.31 (ArO<u>P</u>, s), 110.67 (CH_2O<u>P</u>, s). ^{13}C-NMR (aliphatic carbons, chloroform-*d*): δ 71.62 (<u>C</u>H_2CH_2OP, d, $|^3J(PC)|$ 7 Hz), 69.33 (<u>C</u>H_2OP, d, $|^2J(PC)|$ 18 Hz), 69.14 (<u>C</u>H_2CH_2OAr, s), 68.07 (<u>C</u>H_2OAr, s). ^1H-NMR (chloroform-*d*): δ 7.50–6.60 (m, 28H, P-C_6<u>H</u>$_5$ and C_{12}<u>H</u>$_8$), 3.70 (m, 2H, C<u>H</u>$_2$OAr), 3.58 (m, 2H, C<u>H</u>$_2$O), 3.42 (m, 2H, C<u>H</u>$_2$O), 3.33 (m, 2H, C<u>H</u>$_2$OP).

3.2. 2-(2,2′-$O_2C_{12}H_8$)P(CH_2CH_2O)$_2$–$C_{12}H_8$-2′-P(2,2′-$O_2C_{12}H_8$) (**2**)

A solution of 8.70 g (31.7 mmol) of 2-hydroxy-2′-(1,4-bisoxo-6-hexanol)-1,1′-biphenyl, 15.9 g (63.4 mmol) of 2,2′-biphenylylenephosphochloridite ester and 13.8 ml (99.0 mmol) triethylamine in 150 ml of freshly distilled dichloromethane was stirred under nitrogen for 12 h. Then, the solvent was removed under reduced pressure, and 50 ml of THF was added to the residue. This mixture was stirred at r.t. for 30 min before being filtered to remove the insoluble triethylamine hydrochloride. The filtrate was evaporated to dryness to yield 20.4 g (91.6%) of crude **2** as a viscous, colorless oil that slowly solidified upon standing. $^{31}P\{^1H\}$-NMR (chloroform-*d*): δ 145.21(s, ArO<u>P</u>), 140.79 (s, CH_2O<u>P</u>). ^{13}C-NMR (aliphatic carbons, chloroform-*d*): δ 70.87 (<u>C</u>H_2CH_2OP, d, $|^3J(PC)|$ 3 Hz), 69.28 (<u>C</u>H_2CH_2OAr, s), 68.46 (<u>C</u>H_2OAr, s), 63.81 (<u>C</u>H_2OP, d, $|^2J(PC)|$ 5 Hz). ^1H-NMR (chloroform-*d*): δ 7.51–6.80 (m, 24H, OPO_2C_{12}<u>H_8</u> and C_{12}<u>H_8</u>), 4.05 (m, 2H, C<u>H_2</u>OAr), 3.83 (m, 2H, C<u>H_2</u>O), 3.62 (m, 2H, C<u>H_2</u>O), 3.32 (m, 2H, C<u>H_2</u>OP).

3.3. Mo(CO)$_4${2-$Ph_2PO(CH_2CH_2O)_2$–$C_{12}H_8$-2′-$OPPh_2$} (**3**) (*cis*-**3** and *trans*-**3**)

Solutions of 0.585 g (1.95 mmol) of Mo(CO)$_4$(nbd) in 100 ml of THF and 1.28 g (1.95 mmol) of **1** in 100 ml of THF were added simultaneously and dropwise to 1000 ml of THF over a 2 h period. The mixture was stirred for an additional 18 h and then evaporated to dryness to yield a light brown, oily residue. The residue was taken up in 50 ml of a 1:1 dichloromethane–hexanes mixture, and the resulting solution was treated with 15 g of silica gel. This mixture was filtered, and the silica gel was washed with two, 50 ml portions of a 1:1 dichloromethane–hexanes mixture. The filtrate and washes were combined and evaporated to dryness to yield 1.11 g (66.9%) of **3** as a white powder. Recrystallization from dichloromethane–hexanes gave analytically pure **3**·H_2O as colorless crystals. Anal. Calc. for $C_{44}H_{38}O_9P_2Mo$: C, 60.84; H, 4.41. Found: C, 60.91; H, 4.37%. $^{31}P\{^1H\}$-NMR (freshly prepared chloroform-*d*): major *cis* isomer: δ 146.25 (d, ArO<u>P</u>, $|^2J(PP')|$ 37 Hz), 141.43 (d, CH_2O<u>P</u>, $|^2J(PP')|$ 37 Hz); minor *trans* isomer: δ 162.26 (d, ArO<u>P</u>, $|^2J(PP')|$ 88 Hz), 157.38 (d, CH_2O<u>P</u>, $|^2J(PP')|$ 88 Hz).

3.4. *cis*-Mo(CO)$_4${2-$Ph_2PO(CH_2CH_2O)_2$–$C_{12}H_8$-2′-$OPPh_2$} (*cis*-**3**)

A mixture of 0.585 g (1.95 mmol) of Mo(CO)$_4$(nbd) and 1.284 g (1.95 mmol) of **1** in 100 ml of hexanes was stirred for 2 h at r.t. The mixture was then filtered to yield 1.52 g (91.6%) of crude *cis*-**3** as a light brown solid. $^{31}P\{^1H\}$-NMR (freshly prepared chloroform-*d*): δ 146.25 (d, ArO<u>P</u>, $|^2J(PP')|$ 37 Hz), 141.43 (d, CH_2O<u>P</u>, $|^2J(PP')|$ 37 Hz). ^{13}C-NMR (carbonyl and aliphatic carbons, chloroform-*d*): δ 215.02 (*trans* <u>C</u>O, dd, $|^2J(PC)|$ 29 Hz, $|^2J(P'C)|$ 8 Hz), 214.52 (*trans* <u>C</u>O, dd, $|^2J(PC)|$ 31 Hz, $|^2J(P'C)|$ 9 Hz), 210.40 (*cis* <u>C</u>O, dd, $|^2J(PC)|$ 12 Hz, $|^2J(P'C)|$ 12 Hz), 207.53 (*cis* <u>C</u>O, dd, $|^2J(PC)|$ 10 Hz, $|^2J(P'C)|$ 10 Hz), 70.79 (<u>C</u>H_2CH_2OP, d, $|^3J(PC)|$ 8 Hz), 69.01 (<u>C</u>H_2CH_2OAr, s), 68.81 (<u>C</u>H_2OAr, s), 65.52 (<u>C</u>H_2OP, d, $|^2J(PC)|$ 7 Hz). ^1H-NMR (chloroform-*d*): δ 7.85–6.55 (m, 28H, P–C_6<u>H_5</u> and C_{12}<u>H_8</u>), 4.18 (m, 1H, C<u>H_2</u>OAr), 3.95 (m, 1H, C<u>H_2</u>OAr), 3.77 (m, 1H, C<u>H_2</u>O), 3.53 (m, 2H, C<u>H_2</u>OP), 3.40–3.23 (m, 3H, C<u>H_2</u>O). ν_{CO} (benzene-d_6): 2025, 1931, 1915, 1905 cm^{-1}.

3.5. *cis*-Mo(CO)$_4${2-(2,2′-$O_2C_{12}H_8$)P(CH_2CH_2O)$_2$–$C_{12}H_8$-2′-P(2,2′-$O_2C_{12}H_8$)} (*cis*-**4**)

Solutions of 1.07 g (3.56 mmol) of Mo(CO)$_4$(nbd) in 100 ml of THF and 2.56 g (3.56 mmol) of **2** in 100 ml of THF were added simultaneously and dropwise to 1000 ml of THF over a 2 h period. The mixture was stirred for additional 5 h and then evaporated to dryness to yield a light brown, oily residue. The residue was taken up in a 50 ml of a 1:1 dichloromethane–hexanes mixture. This solution was treated with 15 g of silica gel and then filtered. The silica gel was washed with two, 50 ml portions of a 1:1 dichloromethane–hexanes mixture. The filtrate and washes were combined and evaporated to dryness to yield 3.03 g (93.5%) of *cis*-**4** as a white powder. Recrystallization from ethyl acetate–hexanes gave analytically pure *cis*-**4** as colorless crystals. Anal. Calc. for $C_{44}H_{32}O_{12}P_2Mo$: C, 58.04; H, 3.54. Found: C, 57.94; H, 3.60%. $^{31}P\{^1H\}$-NMR (chloroform-*d*): δ 171.98 (d, ArO<u>P</u>, $|^2J(PP')|$ 48 Hz), 167.85 (d, CH_2O<u>P</u>, $|^2J(PP')|$ 48 Hz). ^{13}C-NMR (carbonyl and aliphatic carbons, chloroform-*d*): δ 210.90 (*trans* <u>C</u>O, dd, $|^2J(PC)|$ 13 Hz, $|^2J(P'C)|$ 9 Hz), 210.21 (*trans* <u>C</u>O, dd, $|^2J(PC)|$ 13 Hz, $|^2J(P'C)|$ 9 Hz), 206.49 (*cis* <u>C</u>O, dd, $|^2J(PC)|$ 14 Hz, $|^2J(P'C)|$ 14 Hz), 205.48 (*cis* <u>C</u>O, dd, $|^2J(PC)|$ 14 Hz, $|^2J(P'C)|$ 14 Hz), 70.30 (<u>C</u>H_2CH_2OP, d, $|^3J(PC)|$ 6 Hz), 69.59 (<u>C</u>H_2CH_2OAr, s), 68.80 (<u>C</u>H_2OAr, s), 67.63 (<u>C</u>H_2OP, d, $|^2J(PC)|$ 11 Hz). ^1H-NMR (chloroform-*d*): δ 8.01–7.00 (m, 24H, P–C_6<u>H_5</u> and C_{12}<u>H_8</u>), 4.54 (ddd, 1H, C<u>H_2</u>OAr), 4.35 (ddd, 1H, C<u>H_2</u>OAr), 4.25 (ddd, 1H, C<u>H_2</u>CH_2OAr), 4.23 (m, 2H, C<u>H_2</u>OP), 4.06 (ddd, 1H, C<u>H_2</u>CH_2OAr), 3.88 (ddd, 1H, C<u>H_2</u>CH_2OP), 3.73 (ddd, 1H, C<u>H_2</u>CH_2OP).

3.6. Reaction of PhLi and *cis*-Mo(CO)$_4$ {2-$Ph_2PO(CH_2CH_2O)_2$–$C_{12}H_8$-2′-$OPPh_2$} (*cis*-**3**)

A solution of *cis*-**3** (0.085 g, 0.10 mmol) in 0.5 ml of

benzene-d_6 was prepared in a 5 mm NMR tube under nitrogen. Phenyllithium (55 μl, 0.10 mmol, 1.8 M in 70:30 cyclohexane–ether) was then added to the tube, and the ^{31}P-NMR spectrum of the solution was taken. During this time, a yellow–orange solid slowly precipitated from the solution. This solid was collected and washed several times with benzene and hexanes to yield 0.072 g (77%) of the crude product as a yellow–orange powder. This compound was extremely reactive, and all attempts to recrystallize this material resulted in its rapid decomposition to give the starting material, *cis*-**3**. $^{31}P\{^1H\}$-NMR (benzene-d_6): δ 174.23 (d, ArO<u>P</u>, $|^2J(PP')|$ 35 Hz), 151.11 (d, CH_2O<u>P</u>, $|^2J(PP')|$ 35 Hz). ν_{CO} (benzene-d_6): 1942, 1873, 1838 cm^{-1}.

3.7. $HgCl_2$-catalyzed cis–trans isomerization of *cis*-$Mo(CO)_4${2-$Ph_2PO(CH_2CH_2O)_2$–$C_{12}H_8$-2′-$OPPh_2$}, *cis*-**3**, and *cis*-$Mo(CO)_4${2-(2,2′-$O_2C_{12}H_8$)$P(CH_2CH_2O)_2$–$C_{12}H_8$-2′-$P(2,2'\text{-}O_2C_{12}H_8)$} (*cis*-**4**)

A solution of either 0.096 g (0.11 mmol) of *cis*-**3** or 0.10 g (0.11 mmol) of *cis*-**4** in 0.5 ml of chloroform-*d* was prepared in a 5 mm, screw-top NMR tube under nitrogen. The head space of the tube was flushed with nitrogen, and both $^{13}C\{^1H\}$- and $^{31}P\{^1H\}$-NMR spectra of the solution were recorded. Then solid $HgCl_2$ (0.3 mg, 0.001 mmol) was added to the solution. After vigorous shaking, a non-quantitative $^{31}P\{^1H\}$-NMR spectrum was acquired, and the *cis* and *trans* resonances were integrated. Additional $^{31}P\{^1H\}$-NMR spectra were taken at 5 min intervals until the *cis*:*trans* ratio reached a constant value. Then, a quantitative $^{31}P\{^1H\}$-NMR spectrum was taken. $^{31}P\{^1H\}$-NMR of **3** (chloroform-*d*): minor *cis* isomer: δ 146.25 (d, ArO<u>P</u>, $|^2J(PP')|$ 37 Hz), 141.43 (d, CH_2O<u>P</u>, $|^2J(PP')|$ 37 Hz); major *trans* isomer: δ 162.26 (d, ArO<u>P</u>, $|^2J(PP')|$ 88 Hz), 157.38 (d, CH_2O<u>P</u>, $|^2J(PP')|$ 88 Hz). $^{31}P\{^1H\}$-NMR of **4** (chloroform-d): minor *cis* isomer: δ 171.98 (d, CH_2O<u>P</u>, $|^2J(PP')|$ 48 Hz), 167.85 (d, ArO<u>P</u>, $|^2J(PP')|$ 48 Hz); major *trans* isomer: δ 191.55 (d, CH_2O<u>P</u>, $|^2J(PP')|$ 237 Hz), δ 178.56 (d, ArO<u>P</u>, $|^2J(PP')|$ 237 Hz).

3.8. X-ray structural analysis of *cis*-$Mo(CO)_4${2-$Ph_2PO(CH_2CH_2O)_2$–$C_{12}H_8$-2′-$OPPh_2$} (*cis*-**3**) and *cis*-$Mo(CO)_4${2-(2,2′-$O_2C_{12}H_8$)$P(CH_2CH_2O)_2$–$C_{12}H_8$-2′-$P(2,2'\text{-}O_2C_{12}H_8)$} (*cis*-**4**)

Hot, saturated dichloromethane–hexanes solutions of both *cis*-**3** and *cis*-**4** were slowly cooled to -10°C to yield X-ray quality, colorless, single crystals of each complex. A suitable crystal of *cis*-**3** was mounted on a glass fiber with epoxy cement under aerobic conditions. A single crystal of *cis*-**4** was mounted in a thin-walled glass capillary under aerobic conditions. Each crystal was mounted and aligned upon an Enraf–Nonius CAD4 single-crystal diffractometer. Details of the data collection of each complex are summarized in Table 1. Standard peak search and automatic indexing routines followed by least squares fits of 25 accurately centered reflections resulted in accurate unit cell parameters for *cis*-**3** and *cis*-**4**.

The analytical scattering factors of each complex were corrected for both $\Delta f'$ and $i\Delta f''$ components of anomalous dispersion. Both structures were solved by the use of Patterson syntheses. Positional and anisotropic thermal parameters for all non-hydrogen

Table 1
Experimental data for crystallographic studies of *cis*-**3** and *cis*-**4**

	cis-**3**	*cis*-**4**
Formula	$C_{44}H_{36}O_8P_2Mo$	$C_{44}H_{32}O_{12}P_2Mo$
Formula weight (Da)	850.65	910.60
Space group	$P\bar{1}$	$Pna2_1$
a (Å)	11.885(3)	18.267(2)
b (Å)	12.410(5)	14.326(2)
c (Å)	15.899(6)	15.277(3)
α (°)	92.98(3)	90
β (°)	99.62(2)	90
γ (°)	116.49(2)	90
Z	2	8
$D_{calc.}$ (g cm^{-3})	1.379	1.513
h_{max}, h_{min}	15, −15	19, −19
k_{max}, k_{min}	16, −16	15, 0
l_{max}, l_{min}	0, −20	16, 0
Diffractometer	Enraf–Nonius CAD4	Enraf–Nonius CAD4
Radiation (Å)	Mo–K_α (λ = 0.71073)	Mo–K_α (λ = 0.71073)
T (K)	298	298
2θ limits (°)	1.0–54.0	2.0–45.0
Reflections measured	9765	5343
Independent reflections measured	9422	2726
Observed reflections	6164 ($F>6\sigma(F)$)	2190 ($F>6\sigma(F)$)
R_{int} (%)	2.02	2.57
Scan type	$\omega-2\theta$	$\omega-2\theta$
Absorption correction	Semi-empirical	Semi-empirical
Absorption coefficient (mm^{-1})	0.45	0.50
Min./max. transmission	0.8050/0.8316	0.7993/0.8154
No. of variables	497	533
Refinement method	Full matrix least-squares	Full matrix least-squares
Quantity minimized	$\Sigma w(F_o-F_c)^2$	$\Sigma w(F_o-F_c)^2$
Weighing scheme (w^{-1})	$\sigma^2(F)+0.0025F^2$	$\sigma^2(F)+0.0005F^2$
Extinction coefficient	NA	$9.5(6)\times10^{-5}$
R (%)	7.17 (all data)/ 3.78(6σ)	3.41(all data)/ 2.19(6σ)
R_w (%)	6.75(all data)/ 4.40(6σ)	3.41(all data)/ 3.05(6σ)
GOF	0.82	0.82
Max. difference peak (e Å^{-3})	0.50	0.31
Max. difference hole (e Å^{-3})	−0.71	−0.27
Max. mean Δ/σ	0.001/0.000	0.001/0.000

Table 2
Selected bond distances (Å) with their estimated S.D. for *cis*-**3** and *cis*-**4**

Atom 1	Atom 2	Distance (Å)	Atom 1	Atom 2	Distance (Å)
cis-**3**					
Mo1	P1	2.530(1)	Mo1	P2	2.508(1)
Mo1	C41	1.985(3)	Mo1	C42	2.011(4)
Mo1	C43	1.988(4)	Mo1	C44	2.054(4)
C45	O5	1.132(6)	C41	O6	1.138(4)
C42	O7	1.147(6)	C43	O8	1.154(6)
P1	O1	1.652(2)	P2	O4	1.627(2)
P1	C17	1.822(4)	P1	C23	1.824(3)
P2	C29	1.824(4)	P2	C35	1.822(3)
C1	O1	1.381(3)	C12	O2	1.362(5)
C13	O2	1.421(6)	C13	C14	1.487(6)
C14	O3	1.411(4)	C15	O3	1.413(5)
C15	C16	1.489(4)	C16	O4	1.436(4)
cis-**4**					
Mo1	P1	2.437(1)	Mo1	P2	2.429(1)
Mo1	C41	2.002(6)	Mo1	C42	2.039(7)
Mo1	C43	2.019(5)	Mo1	C44	2.044(6)
C41	O10	1.148(7)	C42	O11	1.135(8)
C43	O12	1.139(6)	C44	O9	1.126(9)
P1	O1	1.602(4)	P2	O4	1.569(5)
P1	O5	1.611(4)	P1	O6	1.618(4)
P2	O7	1.634(3)	P2	O8	1.612(5)
C1	O1	1.402(6)	C12	O2	1.375(7)
C13	O2	1.437(8)	C13	C14	1.501(9)
C14	O3	1.399(8)	C15	O3	1.405(8)
C15	C16	1.478(9)	C16	O4	1.460(8)

atoms were refined. Hydrogen atoms were not located directly but were input in calculated positions with d (C–H) = 0.96 Å [17]. All calculations were carried out using the Siemens SHELXTL-PC® program package [18]. Selected bond lengths, bond angles and torsion angles are given in Tables 2–4, respectively [19].

3.8.1. *cis*-$Mo(CO)_4\{2\text{-}Ph_2PO(CH_2CH_2O)_2\text{–}C_{12}H_8\text{-}2'\text{-}OPPh_2\}$ (*cis*-**3**)

Unit cell parameters of *cis*-**3** indicate that the crystal belongs to the triclinic crystal system. Intensity statistics clearly favored the centrosymmetric space group $P\bar{1}$ (no. 2) over the noncentrosymmetric space group $P1$. The successful solution and refinement of the crystal structure later confirmed this.

3.8.2. *cis*-$Mo(CO)_4\{2\text{-}(2,2'\text{-}O_2C_{12}H_8)\text{-}P(CH_2CH_2O)_2\text{–}C_{12}H_8\text{-}2'\text{-}P(2,2'\text{-}O_2C_{12}H_8)\}$ (*cis*-**4**)

Unit cell parameters of *cis*-**4** indicate that the crystal belongs to the orthorhombic crystal system. Systematic absences (*h0l* for $h = 2n + 1$, *0k0* for $k = 2n + 1$, *0kl* for $k + l = 2n + 1$, *h00* for $h = 2n + 1$ and *00l* for $l = 2n + 1$) require the space group to be either the noncentrosymmetric $Pna2_1$ (no. 33) or the centrosymmetric *Pnma* (*N*o. 62). Intensity statistics and unit cell volume favored the noncentrosymmetric choice $Pna2_1$. Successful solution and refinement of the crystal structure later confirmed this. The absolute structure was confirmed by an η-refinement procedure with $\eta = 0.9(2)$.

4. Conclusions

Although the unsymmetrical metallacrown ethers, *cis*-$Mo(CO)_4\{2\text{-}Ph_2PO(CH_2CH_2O)_2\text{–}C_{12}H_8\text{-}2'\text{-}OPPh_2\}$ (*cis*-**3**) and *cis*-$Mo(CO)_4\{2\text{-}(2,2'\text{-}O_2C_{12}H_8)P(CH_2CH_2O)_2\text{–}C_{12}H_8\text{-}2'\text{-}P(2,2'\text{-}O_2C_{12}H_8)\}$ (*cis*-**4**), have identical metallacrown ether rings, they have very different reactivities. The differences in reactivities of *cis*-**3** and *cis*-**4** are consistent with more effective interaction of the carbonyl ligands in *cis*-**3** with hard metal cations. The research described in this paper demonstrates that both the conformation of the metallacrown ether ring and the phosphorus substituents affect the interaction of the carbonyl ligands with the hard metal cations.

5. Supplementary material

X-ray crystallographic data for *cis*-**3** and *cis*-**4** including tables of atomic and thermal coordinates, bond lengths and bond angles, torsion angles and least squares planes and ^1H–^1H NOESY and ^1H COSY NMR spectra of *cis*-**4** (21 pages) [19].

Table 3
Selected bond angles (°) with their estimated S.D. for *cis*-**3** and *cis*-**4**

Atom 1	Atom 2	Atom 3	Bond angle (°)	Atom 1	Atom 2	Atom 3	Bond angle (°)
cis-***3***							
P1	Mo1	P2	102.4(1)	P1	Mo1	C41	170.7(1)
P1	Mo1	C42	94.7(1)	P1	Mo1	C43	85.0(1)
P1	Mo1	C44	86.9(1)	P2	Mo1	C41	86.7(1)
P2	Mo1	C42	86.7(1)	P2	Mo1	C43	172.2(1)
P2	Mo1	C44	91.6(1)	Mo1	P2	O4	120.8(1)
Mo1	P2	C29	118.6(1)	Mo1	P2	C35	113.9(1)
Mo1	P1	O1	123.8(1)	Mo1	P1	C17	117.6(1)
Mo1	P1	C23	111.5(1)	P1	O1	C1	125.3(2)
P2	O4	C16	118.4(1)	O4	C16	C15	106.6(2)
O3	C15	C16	107.0(2)	O3	C14	C13	111.3(3)
O2	C13	C14	108.0(3)	O2	C12	C7	116.0(3)
O2	C12	C11	123.7(4)	O1	C1	C2	120.9(2)
O1	C1	C6	118.2(3)				
cis-***4***							
P1	Mo1	P2	91.7(1)	P1	Mo1	C41	173.7(2)
P1	Mo1	C42	90.1(2)	P1	Mo1	C43	89.3(2)
P1	Mo1	C44	90.1(2)	P2	Mo1	C41	94.6(2)
P2	Mo1	C42	88.8(2)	P2	Mo1	C43	178.9(2)
P2	Mo1	C44	86.4(2)	Mo1	P2	O4	115.5(2)
Mo1	P2	O7	120.8(1)	Mo1	P2	O8	112.8(2)
Mo1	P1	O1	117.0(1)	Mo1	P1	O5	112.7(1)
Mo1	P1	O6	119.5(2)	P1	O1	C1	126.1(3)
P2	O4	C16	127.4(4)	O4	C16	C15	108.5(5)
O3	C15	C16	110.2(6)	O3	C14	C13	114.8(6)
O2	C13	C14	107.6(5)	O2	C12	C7	113.4(5)
O2	C12	C11	124.7(6)	O1	C1	C2	117.7(5)
O1	C1	C6	119.6(5)				

Table 4
Selected torsion angles (°) for *cis*-**3** and *cis*-**4**

Atom 1	Atom 2	Atom 3	Atom 4	Torsion angle (°)
cis-***3***				
Mo1	P1	O1	C1	89.9
P1	O1	C1	C6	−127.8
C1	C6	C7	C12	−70.3
C13	O2	C12	C7	−175.0
C12	O2	C13	C14	178.0
O2	C13	C14	O3	67.3
C15	O3	C14	C13	−100.6
C14	O3	C15	C16	166.9
O3	C15	C16	O4	178.2
P2	O4	C16	C15	168.6
Mo	P2	O4	C16	−61.0
cis-***4***				
Mo1	P1	O1	C1	130.6
P1	O1	C1	C6	101.3
C1	C6	C7	C12	63.6
C13	O2	C12	C7	179.4
C12	O2	C13	C14	−171.0
O2	C13	C14	O3	−68.2
C15	O3	C14	C13	−84.4
C14	O3	C15	C16	−167.0
O3	C15	C16	O4	−68.4
P2	O4	C16	C15	145.5
Mo1	P1	O4	C16	165.9

Acknowledgements

The authors thank the Department of Chemistry at The University of Alabama for supporting this research. M. Hariharasarma thanks the Graduate School of The University of Alabama at Birmingham for a Graduate Fellowship.

References

[1] (a) J. Powell, A. Kuksis, C.J. May, S.C. Nyberg, S.J. Smith, J. Am. Chem. Soc. 103 (1981) 5941. (b) J. Powell, S.C. Nyberg, S.J. Smith, Inorg. Chim. Acta 76 (1983) L75. (c) J. Powell, K.S. Ng, W.W. Ng, S.C. Nyberg, J. Organomet. Chem 243 (1983) C1. (d) J. Powell, M.R Gregg, A. Kuskis, P. Meindl, J. Am. Chem. Soc. 105 (1983) 1064. (e) J. Powell, M.R. Gregg, A. Kuksis, C.J. May, S.J. Smith, Organometallics 8 (1989) 2918. (f) J. Powell, A. Kuskis, C.J. May, P.E. Meindl, S.J. Smith, Organometallics 8 (1989) 2933. (g) J. Powell, M.R. Gregg, P.E. Meindl, Organometallics 8 (1989) 2942. (h) J. Powell, A. Lough, F. Wang, Organometallics 11 (1992) 2289.

[2] (a) N.W. Alcock, J.M. Brown, J.C. Jeffery, J. Chem. Soc. Chem. Commun. (1974) 829. (b) N.W. Alcock, J.M. Brown, J.C. Jeffery, J. Chem. Soc. Dalton Trans. (1976) 583. (c) D.H.W. Thewissen, K. Timmer, J.G. Noltes, J.W. Marsman, R.M. Laine, Inorg. Chim. Acta 97 (1985) 143. (d) K. Timmer, D.H.W. Thewissen, Inorg. Chim. Acta 100 (1985) 235. (e) K. Timmer,

D.H.W. Thewissen, J.W. Marsman, Recl. Trav. Chim. Pays-Bas, 107 (1988) 248.
[3] (a) A. Varshney, G.M. Gray, Inorg. Chem. 30 (1991) 1748. (b) A. Varshney, M.L. Webster, G.M. Gray, Inorg. Chem. 31 (1992) 2580. (c) G.M. Gray, C.H. Duffey, Organometallics 13 (1994) 1542. (d) G.M. Gray, F.P. Fish, C.H. Duffey, Inorg. Chim. Acta 246 (1996) 229. (e) G.M. Gray, C.H. Duffey, Organometallics 17 (1998) 3550.
[4] S.J. McLain, F.J. Waller, 1984, US Patent 4 432 904.
[5] M. Hariharasarma, G.M. Gray, J. Chem. Crystallogr. 28 (1998) 297.
[6] (a) J.G. Verkade, L.D. Quin, Phoshorus-31 NMR Spectroscopy in Stereochemical Analysis: Organic Compounds and Metal Complexes, VCH, Weinheim, 1987. (b) Comprehensive Organometallic Chemistry. Vol. 3, Pergamon Press, Oxford, 1982.
[7] H. Friebolin, Basic One- and Two-Dimensional NMR Spectroscopy, Second Enlarged Edition, VCH, Weinheim, 1993.
[8] D.J. Darensbourg, M.A. Murphy, J. Am. Chem. Soc. 100 (1978) 463.
[9] D.J. Darensbourg, R.L. Kump, Inorg. Chem. 17 (1978) 2680.
[10] C.A. Tolman, Chem. Rev. 77 (1977) 313.
[11] J.P. Collman, L.S. Hegedus, J.R. Norton, R.G. Finke, Principles and Applications of Organotransition Metal Chemistry, University Science Books, Mill Valley, California, 1987.
[12] (a) M.J. Baker, K.N. Harrison, A.G. Orpen P.G. Pringle, G.J. Shaw, J. Chem. Soc. Chem. Commun. (1991) 803. (b) M.J. Baker, P.G. Pringle, J. Chem. Soc. Chem. Commun. (1991) 1292.
[13] C.H. Duffey, Ph.D. Thesis, The University of Alabama at Birmingham, 1996.
[14] [*cis*] and [*trans*] were determined by integration of the appropriate peak areas in the quantitative ^{31}P-NMR spectrum.
[15] W. Ehrl, R. Ruck, H. Vahrenkamp, J. Organomet. Chem. 56 (1973) 285.
[16] L.V. Verizhnikov, P.A. Kirpichnikov, Zh. Obshch. Khim. 37 (1967) 1355 (Engl. transl. p. 1281).
[17] M.R. Churchill, Inorg. Chem. 12 (1973) 1213.
[18] Siemens SHELXTL-PC Manual, Release 4.1, Siemens Analytical Instruments, Madison, WI, 1990.
[19] Crystallographic Data has been deposited with the Cambridge Crystallographic Data Center, CCDC No. 11-4974 for *cis*-**3** and CCDC No. 11-4975 for *cis*-**4**. Copies of this information may be obtained free of charge from The Director, CCDC, 12 Union Road, Cambridge, CB1 1EZ UK (Fax: +44-1223-336-033 or e-mail: deposit@ccdc.cam.ac.uk or www://http:www.ccdc.cam.ac.uk).